Nanoscale

Accepted Manuscript

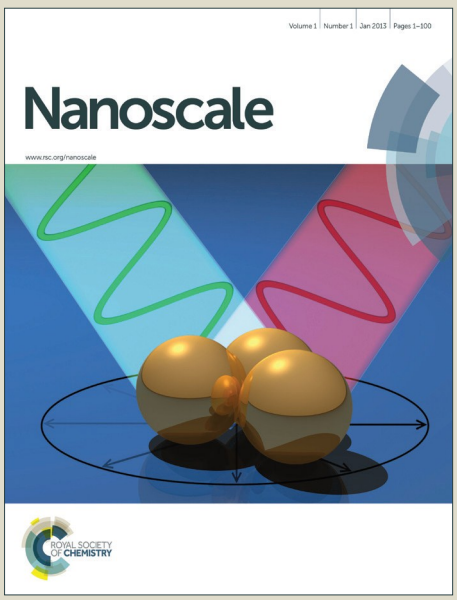

ROYAL SOCIETY OF CHEMISTRY

www.rsc.org/nanoscale

Journal Name

ARTICLE

Facet-Dependent Solar Ammonia Synthesis of BiOCl Nanosheets via a Proton-Assisted Electron Transfer Pathway

Received 00th January 20xx,
Accepted 00th January 20xx

DOI: 10.1039/x0xx00000x

www.rsc.org/

Hao Li, Jian Shang, Jingu Shi, Kun Zhao, and Lizhi Zhang*

Under the pressure of fossil fuels shortage and global climatechange, solar ammonia synthesis becomes more and more urgent forthe N_2 fixation under mild conditions, while itsintrinsic mechanisms still remain unclear. Herein, we demonstrate that kinetic inertia of N_2 can be overcame by using oxygen vacancies (OVs) of BiOCl as the catalytic centers to create lower energy molecular steps, which are amendable for the solar light driven N-N triple bond cleavage via a proton-assisted electron transfer pathway. Moreover, the distinct structures of OVs on different BiOCl facets strongly determine the N_2 fixation pathways by influencing both the adsorption structure and the activation level of N_2. The fixation of terminal end-on bound N_2 on the OVs of BiOCl {001} facets follows an asymmetric distal mode by selectively generating NH_3, while the reduction of side-on bridging N_2 on the OVs of BiOCl {010} facets is more energetically favorable in a symmetric alternating mode to produce N_2H_4 as the main intermediate.

Introduction

Although molecular nitrogen (N_2) as the ultimate source of element N is the major component of the atmosphere on the Earth, most organisms are unable to metabolize N_2 for the synthesis of biomolecules like proteins and nuclei acids. Therefore, all life forms depend on nitrogen fixation, the process through which atmospheric N_2 is transformed to its fully reduced form of ammonia (NH_3) that living organisms can use. Thermodynamically, N_2 fixation is perfectly accessible ($N_{2(g)} + 3H_{2(g)} \rightarrow 2NH_{3(g)}$, $\Delta H_{298\ K} = -92.22$ kJ/mol), but it does not happen spontaneously under ambient conditions. This phenomenon can partly be explained by the stubborn triple bond of N_2 toward dissociation (944 kJ/mol), while is more related to the kinetic inertia of N_2.[1,2] Kinetic reactivity of N_2 for electron transfer and Lewis acid/base reactions is seriously hampered by the lack of a permanent dipole and the large gap (10.82 eV) between the highest occupied molecular orbital (HOMO) and the lowest unoccupied molecular orbital (LUMO) as well as its low proton affinity.[3] For example, direct addition of an electron and a proton to N_2 to yield N_2H requires a large energy input of *ca.* 313.8 kJ/mol, and partial hydrogenation of N_2 to diazene (N_2H_2) and hydrazine (N_2H_4) is rather endothermic (ΔH_f^o = +212.9 kJ/mol for *cis*-N_2H_2 and ΔH_f^o = +95.35 kJ/mol for N_2H_4).[4,5] Those possible intermediates *en route* to full N_2 hydrogenation lie at very high energy levels despite the exothermicity nature of the overall reaction. These thermodynamic analyses reveal that the fixation of N_2 to NH_3 itself is not energy-consuming, while the kinetic routes intrinsically determine the chemical inertness of N_2.

For an overall thermodynamically favored but kinetically impossible uncatalyzed reaction, using catalysts to create energy-accessible intermediary steps is of great importance. The industrial Haber-Bosch process, ranking as one of the most important technological inventions in the 20th century, is a good example to fix N_2. Rather than directly reacting with H_2 up against unsurmountable kinetic limitations, N_2 is dissociatively chemisorbed on the iron-based catalyst (Fe-catalyst) to generate reactive surface-bound nitrides with their subsequent protonation processes being both thermodynamically and kinetically promoted.[6,7] Though producing 150 million tons of NH_3 from $N_2$and H_2 each year, the Haber-Bosch process requires red-hot temperatures (300–550 °C) to realize sufficient reaction efficiency for the large scale production, along with high pressures (15–25 MPa) to shift the equilibrium toward the NH_3 formation (according to Lechatelier's Principle), which consumes about 1.1% of world energy supply with plenty of global greenhouse gas CO_2 being released. On the contrary, the naturally occurring nitrogenase enzyme can do the same work under mild conditions. The most abundant nitrogenase is the Mo-dependent enzyme, whose fundamental steps of N_2 fixation differ from those of Fe-catalyst in the Haber-Bosch process in two ways.[8] First, rather than being directly split at a large energy cost, the N-N triple bond of N_2 is step-by-step hydrogenatively cleaved via multiple proton and electron transfer with the bond order decreasing from 3 to 0.[9,10] Thus, high temperatures are no longer required and the unfavorable

Key Laboratory of Pesticide & Chemical Biology of Ministry of Education, Institute of Environmental Chemistry, College of Chemistry, Central China Normal University, Wuhan 430079, P. R. China
*To whom correspondence should be addressed.
E-mail: zhanglz@mail.ccnu.edu.cn. Phone/Fax: +86-27-6786 7535
Electronic Supplementary Information (ESI) available: [Other experimental details, additional SEM and TEM images, X-ray diffraction patterns (XRD), UV-Vis diffuse reflectance spectra (DRS), and additional data]. See DOI: 10.1039/x0xx00000x

equilibrium of Haber-Bosch process can also be avoided. Second, the iron-molybdenum-sulfur cluster (the FeMo-cofactor) of nitrogenase acts as the catalytic center to bind N_2 and activate (weaken) the triple bond and thus increase its Lewis acid/base reactivity toward the subsequent electron transfer and proton attack.[11,12]

Similar with biological N_2 fixation, photocatalytic N_2 fixation can also be conducted under mild conditions via successive self-excited electron and water-derived proton transfer, while its state-of-the-art efficiency is poor due to the absence of catalytic centers to tune the electronic states of adsorbed N_2 with the thermodynamic driving force only being controlled by electrons.[13] Inspired by the biological N_2 fixation strategy, we recently introduced oxygen vacancies (OVs) on the semiconductor surface to mimic the FeMo-cofactor for N_2 adsorption and N-N triple bond activation, and thus greatly enhanced the kinetic feasibility of photocatalytic N_2 fixation.[14] However, how kinetic inertia of N_2 is overcame after introducing OVs in terms of their influences on the thermodynamics of photocatalytic N_2 fixation, which is evidently involved with several intermediary steps, remains unknown. Moreover, the effects of different semiconductor surfaces' OVs on the N_2 fixation modes have never been studied. Meanwhile, stoichiometry of photocatalytic N_2 fixation includes the combined gain of electrons and protons for the hydrogenative N-N triple bond cleavage.[15-19] Unfortunately, as compared with electron transfer to trigger catalytic reactions, protons have often been ignored, which are supposed to greatly affect the kinetics of interfacial electron transfer by participating in the surface redox reactions.[20-22] Herein, we utilize bismuth oxychloride (BiOCl) of *in situ* OVs generation characteristic under solar light to explore how OVs on different facets will influence both the surface-N_2 interactions and the thermodynamic reaction pathways of N_2 fixation on the surface molecular level, and also study the effects of water-derived protons on the energetics of heterogeneous interfacial electron transfer from the excited BiOCl to the adsorbed N_2.

Results and Discussion

BiOCl is a typical ternary semiconductor with a layered structure interleaved with $[Bi_2O_2]$ slabs and double chlorine atoms slabs, which has attracted increasing attention because of its facet-dependent and defect-related reactivity.[23-25] The BiOCl {001} facets are of a close-packed structure with high density O atoms exposure, while its {010} facets possess an open structure with O, Bi and Cl atoms exposed (Fig. 1a). We prepared single crystalline BiOCl nanosheets exposed with {001} or {010} facets through a simple hydrothermal method and respectively denoted them as BOC-001 and BOC-010 (Fig. S1-S3). It is known that for the photocatalytic utilization of small molecules (O_2, H_2O, and CO_2), both the reactivity and reaction pattern are highly dependent on the first step of the substrates interacting with photocatalysts' surface.[26-29] As for the biological N_2 fixation, the binding of N_2 or its hydrogenated intermediates to different sites of nitrogenase is also structure-related, resulting in different N_2 fixation schemes.[30-32] Therefore, we first investigated the possible adsorption geometry of N_2 on the surfaces of BiOCl by density of functional theory (DFT) calculations. The chemisorption of N_2 on the clean (001) or (010) surface was ruled out because of their weak interaction. Our previous result revealed that the OVs could adsorb and activate N_2 via back donating their available localized electrons to the π antibonding orbital of N_2, while the activated N_2 with negative charges build-up on the N_2 moiety contributed largely to its enhanced Lewis acid/base reactivity. As expected, N_2 can be chemisorbed on the OVs of (001) and (010) surface after generating an OV. Interestingly, their N_2 adsorption geometries are rather different. On the (001) surface, N_2 can be adsorbed on the OV through combining with two nearest Bi atoms in the sublayer to form a terminal end-on bound structure (Fig. 1b). The level of N_2 activation is closely related to the ability of OV to weaken the N-N bond and reflected from both the bond length increase and the bond order decrease. The N-N bond of N_2 adsorbed on the OV of (001) surface, still triple, but exhibits slight activation with the bond length increasing to 1.137 Å, which is between the triple bond length (1.078 Å) of free N_2 and double bond length (1.201 Å) of N_2H_2. Charge density difference revealed that both the exchange and transfer of electrons mainly took place between the OV of (001) surface and N_2. An obvious back transfer of charges from the OV to adsorbed N_2, as depicted by the electron depletion on the OV and electron accumulation on the adsorbed N_2, was the possible reason for the N-N triple bond activation (Fig. S4a). Differently, N_2 exhibited a more stable side-on bridging mode through combining with two nearest Bi atoms in the outer layer and one next nearest Bi atom in the sublayer on the (010) surface (Fig. 1c). It is widely accepted that the side-on bound mode of N_2 is more attractive than the end-on bound mode because the former provides a larger extent of N_2 activation. This point was substantiated by the lower bond order (2) of N_2 adsorbed on the OV of (010) surface and its longer bond length (1.198 Å), which was very close to the value (N_2H_2, 1.201 Å) of N-N double bond. Charge density difference revealed a similar OVs-induced N_2 activation scheme (Fig. S4b). The higher activation level of N_2 adsorbed on the (010) surface could be explained by more electrons transferred from OV to the adsorbed N_2 on (010) surface than those on the (001) surface according to Bader charge analysis (Supporting Information Table S1). Meanwhile, N_2adsorption on the OV of (010) surface is more stabilized by 9.67 kcal/mol than that on the OV of (001) surface (Fig. 1d). Different from the homogenous N_2 fixation by many transition metal-N_2 complexes that have been widely studied for decades, it is rather difficult to experimentally verify the N_2 adsorption structure during this heterogeneous catalytic nitrogen fixation process, although the different OV-N_2 interaction modes could be indirectly reflected by the temperature programmed desorption of N_2 (N_2-TPD) under light irradiation. The N_2-TPD peak location of BOC-010 at higher temperature (282 ^{o}C) confirmed a different structure of higher binding energy for N_2 chemisorbed on the OVs of {010} facets as compared with BOC-001 (Fig. 1e). After solar light

irradiation, both BOC-001 and BOC-010 exhibited a typical OV signal according to low-temperature electron paramagnetic resonance (EPR) analysis and a newly-formed absorption tail in the visible light region of the UV-vis absorbance spectra (inset of Fig. 1e and Fig. S2b).[25]

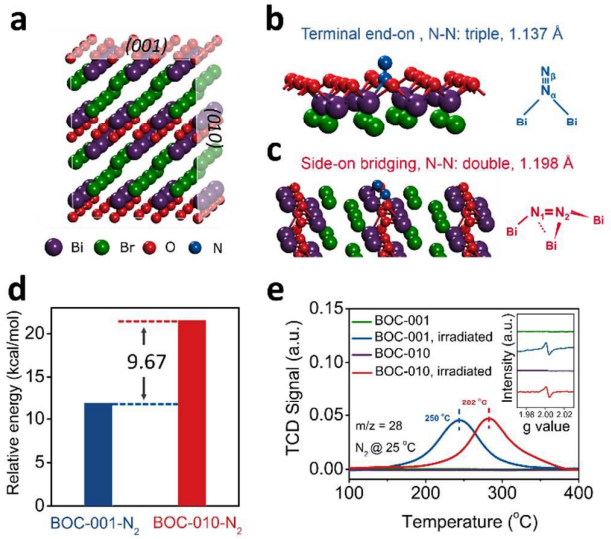

Fig. 1 Adsorption of N_2 on the {001} and {010} facets of BiOCl. (a) Crystal structure of BiOCl and the corresponding cleaved (001) and (010) surface. (b) The terminal end-on adsorption structure of N_2 on (001) surface of BiOCl and (c) the side-on bridging adsorption structure of N_2 on (010) surface of BiOCl. (d) Activation energy of N_2 adsorption on different BiOCl surfaces. (e) N_2-TPD profiles of the as-prepared BiOCl photocatalysts under light irradiation (the inset shows the *in situ*-generated EPR signals corresponded to OVs).

Subsequently, we checked how these different OV-N_2 interaction modes would influence both photoreactivity and reaction pathways of N_2 fixation toward the solar ammonia synthesis. Using H_2O as both the solvent and proton source, BOC-001 could steadily reduce N_2 to NH_3 with a rate of about 1.19 μmol/h under solar light (Fig. 2a). Interestingly, BOC-010 showed an interesting staged NH_3 generation behaviour, as the NH_3 generation rate of BOC-010 after 30 min was 4.62 μmol/h, almost 2.5 times that (1.92 μmol/h) within 30 min (Fig. 2a). Time-dependent high resolution N 1s XPS spectra of the as-prepared BiOCl upon Ar^+ sputtering revealed no residual N (NO_3^-) on the pristine catalysts surface (Fig. S5a-b). Further recyclability test showed both BOC-001 and BOC-010 exhibited sustainable N_2 fixation ability and good photostability (Fig. S5c and S2a). These results ruled out the possibility of N contamination during the synthesis of BiOCl, and thus confirmed the nitrogen in ammonia was from the purged N_2.To understand the effect of surface area on the photoreactivity of BiOCl, we normalized the reaction rates with surface areas and found the normalized NH_3 generation rate ($k'_{BOC\text{-}010}$:0.95 μmol g h^{-1} m^{-2}) of BOC-010 was only half that ($k'_{BOC\text{-}001}$: 1.89 μmol g h^{-1} m^{-2}) of BOC-001 before 30 min (Supporting Information Table S2). After 30 min, $k'_{BOC\text{-}010}$ (2.29 μmol g h^{-1} m^{-2}) was 1.21 times larger than $k'_{BOC\text{-}001}$, even though the OVs generation rate of BOC-001 was much faster than that of BOC-010 (Fig. S5d-f). This indicated that the chemistry of N_2 fixation on the {010} facets was different from that on the {001} counterpart. N_2H_4 and N_2H_2 are believed to be the bona-fide intermediates of nitrogenase based biological N_2 fixation, but scarcely detected or trapped during the photocatalytic N_2 fixation, which conceals the reaction pathways of photocatalytic N_2 fixation.[33,34] In this study, we found that BOC-001 showed a poor reactivity on the reduction of N_2 to N_2H_4 under solar light, but a rapid N_2H_4 formation was observed over BOC-010, which accumulated during the first 30 min of reaction with a normalized N_2H_4 generation rate of 4.14 μmol g h^{-1} m^{-2}, which was almost 2.2 times that of BOC-001 for the NH_3 generation, and then N_2H_4 gradually disappeared (Fig. 2b and Table S2). We therefore called the time range from 0 to 30 min as the induction period of the selective N_2 reduction to N_2H_4 over BOC-010 and interestingly found the accelerated generation of NH_3 over BOC-010 happened just after the induction period of the selective N_2 reduction to N_2H_4. This phenomenon strongly suggested the rapid catalyzed transformation of N_2H_4 to NH_3 during the solar ammonia synthesis of BiOCl. Compared with N_2, N_2H_4 is more inclined to be photocatalytically reduced to NH_3 because of its much weaker N-N single bond. When as-prepared BiOCl nanosheets were allowed to directly react with the freshly-prepared N_2H_4 under solar light, the two kinds of nanosheets exhibited comparable NH_3 generation rates (Fig. 2c). We therefore proposed that the staged NH_3 formation rate of BOC-010 was related to its facet-dependent fast generation of N_2H_4. It is known that the N_2H_4 formation is closely related to the intermediary step of N_2H_2 generation. Unfortunately, N_2H_2 is very unstable and quickly decomposes within seconds in water, we then adopted maleic acid as the N_2H_2 quencher to avoid the further reduction of N_2H_2 because olefinic substrates can oxidize N_2H_2 to N_2 (Fig. 2d).[35] The addition of maleic acid slightly decreased the generation of NH_3 over BOC-001, but largely inhibited the generation of N_2H_4 (after 30 min) and NH_3 (after 120 min) in the case of BOC-010 (Fig. 2e). In contrast, the addition of oxalic acid without a C-C double bond slightly enhanced the N_2 fixation efficiencies of BOC-001 and BOC-010 (Fig. 2e). These results suggested that N_2H_2 was also a possible intermediate of N_2 fixation over BOC-010. We therefore conclude that the $N_2 \rightarrow N_2H_2 \rightarrow N_2H_4 \rightarrow NH_3$ pathway might govern the solar ammonia synthesis of BOC-010, while NH_3 is the selective product throughout the N_2 fixation process over BOC-001 under solar light. This conclusion was further verified by the Fourier transform infrared (FTIR) spectra of the N_2 reduction products (Fig. 2f). Under solar light irradiation for 5 min, several absorption bands were observed with two predominant broad bands ranging from 2600 to 3700 cm^{-1}, which were ascribed to H_2O. Two sharp peaks within these broad bands (3380 cm^{-1} for BOC-001 and 3356 cm^{-1} for BOC-010) were assigned to the $\nu_{N\text{-}H}$ stretching mode and the weak bands at lower wavenumbers (1110 cm^{-1} for BOC-001 and 1079 cm^{-1} for BOC-010) were attributed to the $\sigma_{N\text{-}H}$ bending mode. In comparison with BOC-001, product of BOC-010

possessed a characteristic additional adsorption band at 909 cm^{-1} in the fingerprint region.[35] Moreover, with the reaction time prolonging, the band at 909 cm^{-1} (σ_{N-N}) gradually disappeared along with a steady increase of the band at 3356 cm^{-1} (ν_{N-H}), confirming that N_2H_4 was the intermediate during the solar ammonia synthesis of BOC-010. The quantum yields for the overall NH_3 generation were estimated to be 1.8% for BOC-001 and 4.3% for BOC-010 within 60 min under UV light (λ = 254 nm), respectively (Fig. S6a-b).We then evaluated the possible production of H_2 via the recombination of protons and electrons and found the amount of the generated H_2 was rather negligible, compared with that of generated NH_3 (Fig. S6c). Although OVs might also serve as active sites for H_2O activation and/or dissociation, the H_2O activation and/or dissociation could not compete with the N_2 activation in view of the low N_2 solubility in water. If the activation of N_2 was comparable with that of H_2O in the solution, we would not observe the efficient and continuous ammonia generation in this study, as the amount of H_2O molecules were overwhelmingly larger than that of N_2.

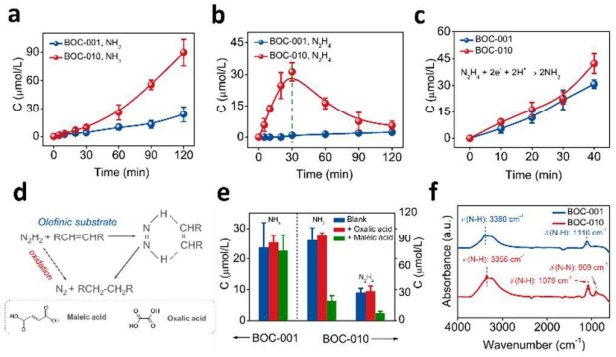

Fig. 2 N_2 Fixation on the {001} and {010} facets of BiOCl. Quantitative determination of the generated (a) NH_3 and (b) N_2H_4 over BiOCl under solar light. (c) Transformation of N_2H_4 to NH_3 over BiOCl under solar light. (d) Schematic illustration of the N_2H_2 quenching process using olefinic substrate. (e) Effect of maleic acid and oxalic acid addition on the solar ammonia synthesis of BiOCl. (f) FTIR spectra of the N_2 reduction products. The error bars arise from values extracted from several measurements on multiple catalysts.

The above theoretical and experimental results revealed that N_2 interacted differently with OVs on distinct facets of BiOCl. We further checked how these different N_2 interaction modes predetermined by OVs would lead to the facet-dependent solar ammonia synthesis of BiOCl. It is widely accepted that fixation of N_2 with an end-on coordination mode typically occurs via a distal mechanism in an asymmetric pathway, wherein continuous hydrogenation are first performed exclusively on the most distant nitrogen atom (N_β) until the first NH_3 is liberated with the N-N triple bond being cleaved (Fig. S7a). Then neighboringnitrogen (N_α) starts another turn of hydrogenation to yield the second NH_3.[36,37] Such a distal mechanism can well explain the hydrogenation of the terminal end-on bound N_2 moiety on the (001) surface of BiOCl, since the polarized N_2 ligand on this close-packed surface exhibits a low coordination number at terminal N_β atom and larger steric hindrance at vicinal N_α, which determine that hydrogenation of the adsorbed N_2 moiety prefers to proceed at the terminal N_β atom rather than the coordinated N_α (Fig. 1b). Moreover, this distal mechanism is not involved with the generation of N_2H_4 or N_2H_2, in good agreement with the experimental observations. As for N_2 with a bridging coordinated structure, its reduction to NH_3, along with generating N_2H_4 or N_2H_2 intermediates, often obeys an alternative mechanism of a symmetric fashion. This alternative mechanism involves the alternative hydrogenation on the N atoms of the coordinated N_2 moiety to generate N_2H_2-level and N_2H_4-level intermediates (Fig. S7b).[38,39] Such an alternative mechanism is exactly applicable to the fixation of side-on bridging bound N_2 moiety on the {010} facets of BiOCl, because the two N atoms (N_1, N_2), both exposed out of the open surface, are charged equally and thus exhibit the same possibility toward hydrogenation (Fig. 1c). More importantly, the existence of N_2H_4 and N_2H_2 during the solar ammonia synthesis of BOC-010 strongly supports this alternative mechanism.

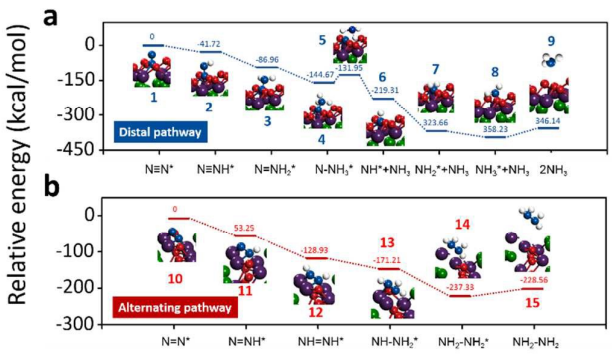

Fig. 3 Free energy change against the reaction coordinate. (a) OV-mediated N_2 fixation on the (001) surface following a distal pathway. (b) OV-mediated N_2 fixation on the (010) surface following an alternating pathway.

A broader DFT study was then carried out to validate the two proposed thermodynamic reaction pathways by calculating relative energy of the possible intermediates. Fig. 3 shows the determined energy level diagram of the N_2 fixation on distinct surfaces of BiOCl. For the N_2 fixation on the OV of BiOCl (001) surface, the distal mechanism involves preferential hydrogenation of **1** (N≡N*) on the terminal N_β, including the first crucial step of hydrogenation at terminal N_β to yield **2** (N≡NH*), which is the most difficult step of the whole process and strongly endergonic for free N_2 (Fig. 3a). As soon as N_2 is adsorbed on the OV of (001) surface, such a hydrogenation step becomes rather exergonic with free energy change of 41.72 kcal/mol and the N-N triple bond being elongated from 1.137 Å to 1.227 Å (Fig. S8a and S8b). The next hydrogenation to produce **3** (N=NH_2*) is also found to be exergonic by 45.24 kcal/mol, accompanying with the reduction of N-N triple bond to double bond (Fig. S8b). Further hydrogenation of **3**to

generate hydrazidium intermediate **4** (N-NH_3*) of single N-N bond is calculated to be exergonic by 57.71 kcal/mol. The intermediate **4** exhibits a quite elongated N-N bond length of 1.492 Å and is thus considered to be highly activated, as evidenced by the small energy input of 12.72 kcal/mol to cleave the N-N bond. After the N-N bond splitting, nitrido intermediate **5** (N* + NH_3) is formed with simultaneously releasing the first NH_3molecule. The intermediate **5** is very susceptible to further hydrogenation owing to the strongly exergonic character of its transformation to **6** (NH*) (87.36 kcal/mol). The subsequent hydrogenation of **6** to yield **7** (NH_2*) is more energy accessible, as calculated to be exergonic by 104.35 kcal/mol. The final hydrogenation of **7** to form surface bound ammine intermediate **8** (NH_3*) is exergonic by 34.57 kcal/mol. Desorption of the second NH_3 molecule to reconstitute the initial chemical state of (001) surface is of great significance, as only through this process can the OV become electron rich again to bind N_2 and thus initiate another catalytic cycle.[40-42] Dissociation of **8** under the reformation of initial (001) surface **9** to release the second NH_3 for the whole catalytic cycle completion is calculated to be endergonic with free energy change of 12.09 kcal/mol. We also interestingly found that the N_α–Bi bond lengths gradually decreased (Fig. S8c), when hydrogenation was exclusively performed on the terminal N_β. This bond decrease indicates that the vicinal N_α tends to diffuse into the BiOCl (001) surface to increase the steric hindrance against the proton attack, disfavoring the alternative hydrogenation at N_α to generate N_2H_2 or N_2H_4. However, after N-N bond is cleaved and N_α starts undergoing hydrogenation, the N_α–Bi bonds length in turn gradually increases, indicating the hydrogenated N_α moiety is highly inclined to desorb from the (001) surface, especially for the fully hydrogenated nitrogen moiety of **8** that almost diffuses out of the BiOCl (001) surface (Fig. S8c).

As for the fixation of N_2 on the OV of BiOCl (010) surface via the alternating mechanism, first hydrogenation of **10** (N=N*) to yield **11** (N=NH*) is calculated to be exergonic with free energy change of 53.25 kcal/mol, along with double bond being increased from 1.198 Å to 1.220 Å (Fig. 3b and Fig. S9a and S9b). Second hydrogenation of **11** at another N is exergonic by 75.68 kcal/mol, generating the important N_2H_2-level intermediate **12** (NH=NH*). Further reduction of **12** to yield **13** (NH-NH_2*) is calculated to be exergonic by 42.28 kcal/mol, reducing the N-N double bond to single one and stretching its bond length to 1.448 Å, almost the same as the N-N length (1.450 Å) of free N_2H_4. On the basis of the instant elongated N_1-Bi_3 bonds length, intermediate **13** exhibits a general tendency to leave the (010) surface (Fig. S9c). As expected, the last hydrogenation of **13** leads to the formation of **14** containing a nearly free N_2H_4* molecule in an exothermic process with free energy change of 66.12 kal/mol. Remarkably, energy expenditure of N_2 fixation on the (010) surface involved with the N_2H_4 desorption to refresh the surface **15** is 8.77 kcal/mol, smaller than that (12.09 kal/mol) of overall N_2 fixation on (001) surface. Actually, it is highly instructive to compare the energetics of N_2 fixation on the OV of BiOCl surface with the free (uncatalyzed) N_2 fixation reactions. Different from the OV-mediated N_2 fixation, the uncatalyzed N_2 fixation is up against unsurmountable barriers toward the intermediate of either N_2H_2 or N_2H_4, clarifying the indispensable roles of OVs in creating these accessible molecular steps to a thermodynamically favored but kinetically impossible uncatalyzed N_2 fixation (Fig. S10).

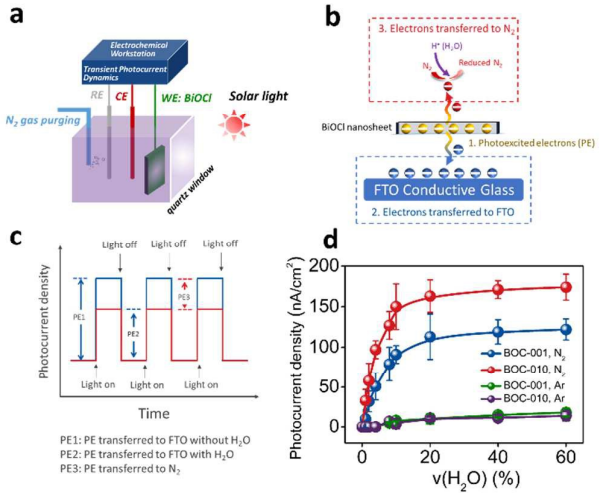

Fig. 4 Studying the effect of proton on the interfacial electron transfer during N_2 fixation. (a) The designed electrochemical reaction cell to record transient photocurrent responses. The working electrode (WE) was prepared by dip coating BiOCl nanosheets onto the FTO conductive glass. Pt foil and saturated calomel were respectively used as counter electrode (CE) and reference electrode (RE). The electrolyte was prepared by dissolving 0.01 mol sodium perchlorate into a mixture of CH_3CN and H_2O. During the reactions, the N_2 was kept purging into this cell. Schematic illustration of (b) the electron transfer scheme in this micro-reaction system and (c) the output image of transient photocurrent responses which can indirectly reflect the electrons being transfer to reactant of N_2. (d) The photocurrent response of PE3 reflecting the electron transfer from excited BiOCl to N_2 as a function of the proportion of water in CH_3CN. The Ar purging was used for comparison. The error bars arise from values extracted from several measurements on multiple catalysts.

For each elementary N_2 reduction step via either the distal or alternating mechanism, it requires the transfer of an electron and a proton.[36-39] Although electron transfer is the rate-limiting step to trigger catalytic N_2 fixation, our hydrogen/deuterium (H/D) kinetic isotope study with using D_2O as the solvent revealed that kinetic isotope effects (KIE) of solar ammonia synthesis over BiOCl were 1.30 ± 0.07 for BOC-001 and 1.87 ± 0.11 for BOC-010, respectively. Such KIE values excluded the possibility of concerted proton-coupled electron transfer, but suggested the non-negligible influence of proton transfer on interfacial redox reactions.[43] To clarify how the proton might affect the interfacial redox reactions, we designed an electrochemical reaction cell of a saturated N_2 environment, in which the kinetics of surface N_2 fixation can be reflected by the dynamics of transient photocurrent

responses of excited BiOCl (Fig. 4a). In this micro-reaction system, most survived photoexcited electrons (PE1) of BiOCl nanosheets should be transferred to the FTO glass in the non-protic electrolyte CH_3CN. If CH_3CN is partially replaced with H_2O, a competitive photoexcited electron transfer to the adsorbed N_2 will result in the decreased photoexcited electrons (PE2) transferred to FTO glass (Fig. 4b).[14] Theoretically, photoexcited electrons (PE3) transferred from BiOCl to the adsorbed N_2 equal to PE1 minus PE2, which should be closely related to the concentration of protons in CH_3CN and reflected by the difference of the average transient photocurrent responses in the presence of different proportional H_2O (Fig. 4c). We first tried to barricade the direct interaction between OVs and adsorbed N_2 by coating the pristine BiOCl electrodes with a layer of SiO_2. As expected, we observed an almost linear but slow increase of the electrons being transferred from excited BiOCl-SiO_2 to N_2 (PE3 responses) for the two kinds of nanosheets along with increasing the H_2O concentration in CH_3CN from 0% to 10% (Fig. S11). However, for the pristine BiOCl electrodes, much sharper PE3 responses were observed and could be described by a sigmoidal curve, defined by a sudden rise and a final equilibrium, along with increasing the H_2O concentration (Fig. 4d). After N_2 was replaced with Ar, the change of PE3 became tiny, which might be simply arisen for the conductivity change caused by different ratios of H_2O/CH_3CN. The more prominent sigmoidal curves of PE3 responses in the case of the pristine BiOCl electrodes revealed the presence of protons significantly accelerated the transfer of electrons from the excited BiOCl to the adsorbed N_2, if OVs were directly interacted with adsorbed N_2. Notably, protons are supposed to be more critical in the N_2 fixation reactions on the {010} facets, as reflected by their higher PE3 response, consistent with their larger kinetic isotope effect and less energy-demanded N_2 fixation nature as compared with those of {001} facets (Fig. 4d). We believe this interesting proton assisted electron transfer process during the solar ammonia synthesis is positively related to the level of N_2 activation on the OVs, as the activated N_2 with more negative charge build-up (such as N_2 on the OV of BOC-010) exhibits stronger Lewis basicity toward the proton attack, and thus facilitates the successive electron transfer for the N_2 fixation and avoids the local charge accumulation.[44,45] Therefore, proton-assisted electron transfer can be a more favorable reaction pathway than a strict sequence of individual electron and proton transfer. To verify this point of view, we used Degussa TiO_2 (P25) without *in situ*-OV generation property for comparison (Fig. S12). Without OVs to activate N_2, the KIE of P25 was close to 1 (1.07 ± 0.06), indicating that the proton transfer did not affect the interfacial surface redox reactions during P25 photocatalysis. Meanwhile, with increasing the H_2O concentration in CH_3CN from 0% to 10%, a linear increase of the electrons being transferred from the excited P25 to N_2 (PE3 responses) was observed in the designed electrochemical reaction cell, which was significantly different from the fast-increasing sigmoidal curves of PE3 responses in the case of BiOCl. This difference suggested that the electron-transfer process during the N_2 fixation on P25 surface was not assisted by the proton transfer (Fig. S12e). Moreover, P25 exhibited a much lower surface area normalized N_2 fixation rate (Table S2). Therefore, we propose that N_2 activation on OVs increases the Lewis basicity of adsorbed N_2 to favor the subsequent proton attack, and thus facilitates the successive electron transfer for the N_2fixation and avoids the local charge accumulation.

Conclusions

In summary, we have clarified the indispensable roles of OVs on the adsorption and activation of N_2 to enhance the kinetic feasibility of N_2 fixation by creating lower molecular steps amendable for the N-N triple bond cleavage via a proton-assisted electron transfer. We have also demonstrated that semiconductor-based photocatalytic and nitrogenase-based biological N_2 fixation systems share similarities on the aspect of catalytic center structures, which significantly influence the substrate-reactant interaction modes and determine the N_2 fixation mechanistic pathways. These findings are crucial for the ultimate establishment of a truly catalytic system for solar ammonia synthesis.

Experimental Section

Chemicals. All chemicals used were purchased from Sinopharm Chemical Reagent Co., Ltd. (Shanghai, China) and were of analytical grade and used without purification.

Preparation of BiOCl single-crystalline nanosheets. BiOCl single-crystalline nanosheets were prepared by the method reported by our group.[46] In a typical procedure, 1 mmol of $Bi(NO_3)_3{\cdot}5H_2O$ was added into 18 mL distilled water containing 1 mmol of KCl. Then the pH value was adjusted to 1 or 6 under continuous stirring. The above solutions were poured into an autoclave and was allowed to be heated at 220 °C for 24 h under autogenous pressure. The resulting precipitates after being air cooled to room temperature were collected and washed with deionized water for 6 times and dried at 60 °C for 24 h in air. The BiOCl nanosheets with {001} facets exposed obtained under pH = 1 were denoted as BOC-001 and the BiOCl nanosheets with {010} facets exposed obtained under pH = 1 were denoted as BOC-010.

DFT theoretical calculation. All calculations were performed using the first-principles density of functional theory (DFT) + *U* calculations with the exchange-correlation energy functional, which were described by generalized gradient approximation with the by Perdew-Burke-Ernzerhof (PBE) exchange-correlation function.[47] (1×1) surface was applied to test the thickness of the atomic layers of the slabs for all the models, which was implemented by the CASTEP code in which plane-wave pseudopotential approach and ultrasoft pseudopotentials were employed for all the atoms with a kinetic energy cutoff of 380 eV.[48, 49] All the structures were relaxed to an energy convergence of 10^{-5} eV/atom and a force convergence of 0.03 eV/Å. A Monkhorst-Pack mesh for BOC bulk, BOC-001 and BOC-010 were 4 × 4 × 2, 4 × 4 × 1 and 2 × 4

× 1, respectively.[50] To simulate the N_2 activation on the BiOCl surfaces, a (2 × 2) supercell was used and enabled by a VASP code in which the projector augmented wave (PAW) method represented the electron-ion interaction with a kinetic energy cutoff of 520 eV.[51, 52] During optimizations, the energy and force converged to 10^{-5} eV/atom and 0.02 eV/Å, respectively. The k-points were 2 × 2 × 1 for the BOC-001 supercell and 2 × 3 × 1 for the BOC-010 supercell. The slabs of BOC-001 and BOC-010 were convergent at 11 and 7 atomic layers, respectively. Energy of the respective surface-bound intermediates and free molecules are corrected by their corresponding zero point energy, which are provided in the in Table S3.

Solar ammonia synthesis. All the solar ammonia synthesis experiments were conducted at ambient temperature using a 500 W Xenon lamp to simulate the solar light. Typically, 0.05 g of photocatalyst was added into 75 mL of double distilled water in a reactor. In order to totally erase the influence of photoexcited holes on the electron dynamics, 25 mL of CH_3OH was added as the hole scavenger. The reactor was equipped with water circulation in the outer jacket in order to maintain at room temperature of 25 ^{o}C. The mixture was continuously stirred in the dark and under visible light with high-purity N_2 bubbled at a flow rate of 60 mL/min for 30 min and 120 min, respectively. Five milliliters of the solution was taken out at certain time and centrifuged to remove the photocatalyst. Concentration of ammonia and hydrazine were spectrophotometrically determined by Nessler's reagent and para-(dimethylamino) benzaldehyde, respectively.[53] KIE values were defined as the ratio of the k_{D2O} into the k_{H2O}, in which k_{D2O} and k_{H2O} are respective the NH_3 generation rate of BOC-001 (BOC-010) in D_2O and H_2O.

Acknowledgements

This work was supported by National Natural Science Funds for Distinguished Young Scholars (Grant 21425728), National Basic Research Program of China (973 Program) (Grant 2013CB632402), and National Natural Science Foundation of China (Grant 21177048 and 51472100).

Notes and references

1 M. W. Chase Jr., *NIST-JANAF Thermochemical Tables*, 4 thed; American Chemical Society and American Institute of Physics Press: New York, 1998.
2 A. E. Shilov, *Russ. Chem. Bull.*, 2003, **52**, 2555.
3 C. G. Zhan, J. A. Nichols and D. A. Dixon, *J. Phys. Chem.*, *A* 2003, **107**, 4184.
4 H. P. Jia and E. A. Quadrelli, *Chem. Soc. Rev.*, 2014, **43**, 547.
5 V. Smil, *Nature,* **1999**, *400*, 415.
6 G. Ertl, *Angew. Chem. Int. Ed.,* 2008, **47**, 3524.
7 G. A. Somorjai and Y. Li, *Proc. Natl. Acad. Sci. U. S. A.*, 2011, **108**, 917.
8 V. Smil, *Enriching the Earth: Fritz Haber, Carl Bosch, and the Transformation of World Food Production*; MIT Press: Cambridge, MA, 2004.
9 R. N. F. Thorneley and D. J. Lowe, *Biochem. J.*, 1984, **224**, 887.
10 B. K. Burgess and D. J. Lowe, *Chem. Rev.*, 1996, **96**, 2983.
11 D. R. Dean, J. T. Bolin and L. Zheng, *J. Bacteriol.*, 1993, **175**, 6737.
12 S. C. Lee and R. H. Holm, *Chem. Rev.*, 2004, **104**, 1135.
13 D. Zhu, L. Zhang, R. E. Ruther and R. J. Hamers, *Nat. Mater.*, 2013, **12**, 836.
14 H. Li, J. Shang, Z. H. Ai and L. Z. Zhang, *J. Am. Chem. Soc.*, 2015, **137**, 6393.
15 G. N. Schrauzer and T. D. Guth, *J. Am. Chem. Soc.*,1977, **99**, 7189.
16 M. M. Khader, N. N. Lichtin, G. H. Vurens, M. Salmeron and G. A. Somorjai, *Langmuir*, 1987, **3**, 303.
17 N. N. Rao, S. Dube and P. Natarajan, *Appl. Catal. B Environ.*, 1994, **5**, 33.
18 O. Linnik and H. Kisch, *Photochem. Photobiol. Sci.*, 2006, **5**, 938.
19 W. Zhao, J. Zhang, X. Zhu, M. Zhang, J. Tang, M. Tan and Y. Wang, *Appl. Catal. B Environ.*, 2014, **144**, 468
20 C. Chen, T. Shi, W. Chang and J. Zhao, *Chem. Cat. Chem.*, 2015, **7**, 724.
21 J. N. Schrauben, R. Hayoun, C. N. Valdez, M. Braten, L. Fridley and J. M. Mayer, *Science*, 2012, **336**, 1298.
22 C. N. Valdez, M. Braten, A. Soria, D. R. Gamelin and J. M Mayer, *J. Am. Chem. Soc.*, 2013, **135**, 8492.
23 J. Jiang, K. Zhao, X. Y. Xiao and L. Z. Zhang, *J. Am. Chem. Soc.*, 2012, **134**, 4473.
24 K. Zhao, L. Z. Zhang, J. J. Wang, Q. X. Li, W. W. He and J. J. Yin, *J. Am. Chem. Soc.*, 2013, **135**, 15750.
25 H. Li, J. G. Shi, K. Zhao and L. Z. Zhang, *Nanoscale*, 2014, **6**, 14168.
26 M. Setvín, U. Aschauer, P. Scheiber, Y. F. Li, W. Hou, M. Schmid, A. Selloni and U. Diebold, *Science*, 2013, **341**, 988.
27 S. Tan, Y. Ji, Y. Zhao, A. Zhao, B. Wang, J. Yang and J. G. Hou, *J. Am. Chem. Soc.*, 2011, **133,** 2002.
28 J. Lee, D. C. Sorescu and X.Deng, *J. Am. Chem. Soc.*, 2011, **133**, 10066.
29 C. Zhang and P. J. D.Lindan, *J. Chem. Phys.*, 2003, **118**, 4620.
30 R. N. F. Thorneley and D. J. Lowe, *J. Biol. Inorg. Chem.*, 1996, **1**, 576.
31 B. M. Hoffman, D. Lukoyanov, Z. Y. Yang, D. R. Dean and L. C. Seefeldt, *Chem. Rev.*, 2014, **114**, 4041.
32 J. B. Howard and D. C. Rees, *Proc. Natl. Acad. Sci.*, 2006, **103**, 17088.
33 B. M. Barney, J. McClead, D. Lukoyanov, M. Laryukhin, T. Yang, D. R. Dean, B. M. Hoffman and L. C.Seefeldt, *Biochemistry*, 2007, **46**, 6784.
34 B. Hinnemann and J. K. Nørskov, *J. Am. Chem. Soc.,* 2004, **126**, 3920.
35 C. T. Johnston and K. Intercalate, *Spectroscopic Characterization of Minerals and Their Surfaces* Chapter 22, pp 432–454.
36 C. J. Pickett, *J. Biol. Inorg. Chem.*, 1996, **1**, 601.
37 R. R. Schrock, *Acc. Chem. Res.*, 2005, **38**, 955.
38 Dilworth, M. J. and R. N. F. Thorneley, *Biochem. J.*, 1981, **193**, 971.
39 B. M. Hoffman, D. R. Dean and L. C. Seefeldt, *Acc. Chem. Res.*, 2009, **42**, 609.
40 Z. Cao, Z. Zhou, H. Wan and Q. Zhang, *Int. J. Quantum Chem.*, 2005, **103**, 344.
41 F. Neese, *Angew. Chem. Int. Ed.*, 2005, **45**, 196.
42 S. Schenk, B. Kirchner and M. Reiher, *Chem. Eur. J.*, 2009, **15**, 5073.
43 M. Khan, *Angew. Chem. Int. Ed.*, 1988*,* **27**, 923.
44 J. J. Warren, T. A. Tronic and J. M. Mayer, *Chem. Rev.*, 2010, **110**, 6961.
45 D. R. Weinberg, C. J. Gagliardi, J. F. Hull, C. F. Murphy, C. A. Kent, B. C. Westlake, A. Paul, D. H. Ess, D. G. McCafferty and T. J. Meyer, *Chem. Rev.,* 2012, **112**, 4016.
46 H. Li and L. Z. Zhang *Nanoscale*, 2014, **6**, 7805.

47 J. P. Perdew, K. Burke and M. Ernzerhof, *Phys. Rev. Lett.*, 1996, **77**, 3865.
48 M. D. Segall, P. L. D. Lindan, M. J. Probert. C. J. Pickard. P. J. Hasnip, S. J. Clark and M. C. Payne, *J. Phys. Cond. Matt.*, 2002, **14**, 2717.
49 D. Vanderbilt, *Phys. Rev. B*, 1990, **41**, 7892.
50 H. J. Monkhorst and J. D. Pack, *Phys. Rev. B*, 1976, **13**, 5188.
51 G. Kresse and J. Furthmuller, *Phys. Rev. B*, 1996, **54**, 11169.
52 G. Kresse, and D. Joubert, *Phys. Rev. B*, 1999, **59**, 1758.
53 G. W. Watt and J. D. Chrisp, *Anal. Chem.*, 1952, **24**, 2006.